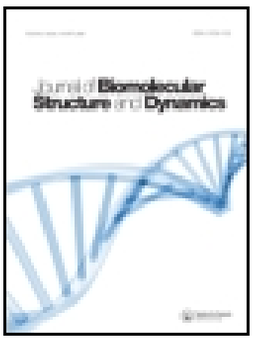

Taylor & Francis
Taylor & Francis Group

Journal of Biomolecular Structure and Dynamics

ISSN: 0739-1102 (Print) 1538-0254 (Online) Journal homepage: https://www.tandfonline.com/loi/tbsd20

Transient decondensation of chromatin in liver nuclei of rats treated with tannic acid

Anush L. Asatryan, Karine S. Matinyan, Irina G. Artsruni, Emil S. Gevorgyan, Ara P. Antonyan & Poghos O. Vardevanyan

To cite this article: Anush L. Asatryan, Karine S. Matinyan, Irina G. Artsruni, Emil S. Gevorgyan, Ara P. Antonyan & Poghos O. Vardevanyan (2019): Transient decondensation of chromatin in liver nuclei of rats treated with tannic acid, Journal of Biomolecular Structure and Dynamics, DOI: 10.1080/07391102.2019.1664332

To link to this article: https://doi.org/10.1080/07391102.2019.1664332

Accepted author version posted online: 05 Sep 2019.
Published online: 15 Sep 2019.

JOURNAL OF BIOMOLECULAR STRUCTURE AND DYNAMICS
https://doi.org/10.1080/07391102.2019.1664332

Taylor & Francis
Taylor & Francis Group

LETTER TO THE EDITOR

Transient decondensation of chromatin in liver nuclei of rats treated with tannic acid

Anush L. Asatryan, Karine S. Matinyan, Irina G. Artsruni, Emil S. Gevorgyan, Ara P. Antonyan and Poghos O. Vardevanyan

Department of Biophysics, Faculty of Biology, Yerevan State University, Yerevan, Armenia

Communicated by Ramaswamy H. Sarma

ARTICLE HISTORY Received 19 July 2019; Accepted 22 August 2019

Introduction

PARP 1 is chromatin-associated enzyme that is responsible for post-translational modification of proteins involved in DNA repair, replication, regulation of chromatin dynamics and transcription (Gupte, Liu, & Kraus, 2017). This abundant nuclear protein has a multidomain structure with different functional activities: N-terminal end of PARP 1 molecule is responsible for binding to chromatin, ssDNA and dsDNA. C-terminal end of the enzyme molecule comprises catalytic pocket, which consists of helical subdomains implicated in allosteric regulation of enzymatic activity, NAD^+-binding subdomain, where NAD^+ is cleaved to nicotine amide and ADP-ribose moiety, and subdomain which is responsible for ADP-ribose transferase activity (Longelier, Planck, Roy, & Pascal, 2012). PARP 1 activity dramatically increases after binding to ssDNA, dsDNA or DNA cruciform, and enzyme performs sequential addition of ADP-ribose units mainly to itself and to adjacent protein molecules. PARP 1-modified proteins harbor long branched chains of poly(ADP-ribose)moieties, which substantially affect the net negative charge of an acceptor molecule. Recently, transient and reversible poly (ADP-ribos)ylation of DNA by PARP 1 at phosphorylated ends was demonstrated.

Poly-ADP-ribose chains attached to DNA are removed by PARG, one of the key 'eraser' proteins involved in cellular poly(ADP-ribose) polymer (PAR) turnover.

PAR metabolism plays a significant role in the determination of chromatin dynamics and chromatin-associated functions (Karlberg, Langelier, Pascal, & Schüler, 2013). Mounting data come to show that modulations of PAR metabolism could be induced by different extra- and intra-cellular signals, targeting enzymatic activities of the main players responsible for PAR synthesis and catabolism in cell nuclei: PARP 1 and PARG. It was documented that tannic acid (TA) a plant-derived polyphenolic substance which is employed in medicinal purposes for centuries display anti-mutagenic, anti-oxidant and anti-cancer activities (Zhang, Li, Kim, Hagerman, & Lü, 2009). In 1989 Tanuma et al revealed dose-dependent inhibitory effect of TA on purified PARG (Tanuma, Sakagami, & Endo, 1989). The number of works devoted to tannins and PARG has been performed with the tannin cocktail gallotannin or TA, which represents a mix of esters of gallic acid with glucose. In 1998, it was documented that TA provided sensitization against DNA cleavage activity of S1 nuclease.

ADP-ribosylation of the nuclear DNA revalidates the roles of PARG and PARP activities in the regulation of chromatin dynamics and functions. To study whether treatment of hall animals with TA via i.p. injection into rats could alter chromatin condensation in liver cell nuclei, we examine chromatin accessibility by structure-dependent assay (Widlak, Li, Wang, & Garrard, 2000). In this purpose, we employ artificially activated intra-nuclear apoptotic Ca^{2+}/Mg^{2+} endonuclease (CME) to evaluate chromatin degradation in the liver cell naked nuclei. Taking into account that chromatin structure could be modulated by direct interaction of TA with DNA, in present study, we intend to examine calf thymus DNA melting profiles in the presence of TA.

Materials and methods

Animals

Animals were treated according to regulations of Committee for Bioethics of Yerevan State University.

Albino inbred male rats were used throughout experiments. Animals were obtained from a stock of animal house of faculty of Biology, Yerevan State University. Rats were housed in laboratory conditions ($20 \pm 2\,^{\circ}C$) with a light/dark cycle, fed with commercial rat feed ad libitum and were given free access to water. Animals were standardized by weight (100 g) and divided into two experimental groups. Group 1: control group-injected intra-peritoneal (i.p.) with saline. Group 2-rats injected i.p. with 100 mg/kg TA. TA was dissolved in saline with the respective concentrations. In different time intervals after TA treatment (2, 24, and 48 h), rats were sacrificed under light ether anesthesia by decapitation. The procedures were approved by the National Centre of Bioethics (Armenia) and performed according to the International Recommendations (CIOMS, 1985) guidelines.

All reagents were purchased from Sigma-Aldrich (St. Louis, MO).

CONTACT Poghos O. Vardevanyan p.vardevanyan@ysu.am

Table 1. Relative content (%) of DNA fragments of different length isolated from nuclei incubated in the presence of divalent ions for different time intervals. DNA content per lane in gel was set as 100%. $p < 0.05$.

Fragment length	15 min incubation with 6mM $MgCl_2$ and 1 mM Ca Cl_2	30 min incubation with 6mM $MgCl_2$ and 1 mM Ca Cl_2	60 min incubation with 6mM $MgCl_2$ and 1 mM Ca Cl_2
>1000 b.p.	90.9 ± 1.0	78.8 ± 0.3	29.5 ± 2.7
1000–200 b.p.	7.8 ± 0.02	16.2 ± 0.2	29.5 ± 0.5
<200 b.p.	1.3 ± 0.01	5.0 ± 0.02	41 ± 1.0

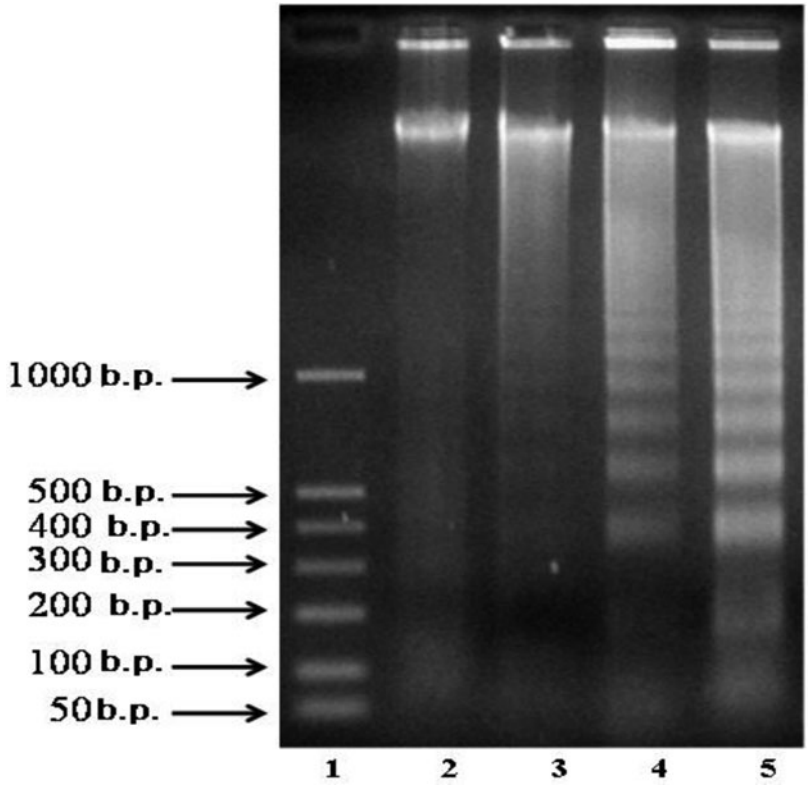

Figure 1. Effect of divalent ions on DNA internucleosomal fragmentation in rat liver nuclei isolated from rats of control group. Lanes: 1 – commercially available DNA1adder, 2 – isolated nuclei were incubated in media which did not contain Mg^{+2} and Ca^{+2} ions, 3 – isolated nuclei were incubated 15 min in media containing 6 mM $MgCl_2$ and 1 mM $CaCl_2$, 4 – isolated nuclei were incubated 30 min in media containing 6 mM $MgCl_2$ and 1 mM $CaCl_2$, 4 – isolated nuclei incubated 60 min in media containing 6 mM $MgCl_2$ and 1 mM $CaCl_2$.

Nuclei isolation

Albino inbred male rats (6 weeks old) were used throughout experiments. The animals were standardized by weight to 100 g and killed in different time intervals under light ether anesthesia by decapitation. Livers were collected and nuclei were isolated according to Hewish and Burgoyne (Hewish, & Burgoyne, 1973). Sucrose solutions utilized throughout nuclei isolation procedure were buffered with 20 mM Tris containing 15 mM NaCl, 60 mM KCl, 0.15mM spermine, and 0.5 mM spermidine at pH 7.4.

PARP1 activity determination

The enzymatic assay for PARP 1 activity was performed according to the original method based on the chemical determination of NAD^+ concentration in PARP assay buffer (Putt & Hergenrother, 2004). The original method was adapted in purpose to quantify NAD^+ consumed by naked nuclei in 10 min from incubation media. Briefly, nuclei were gently suspended in PARP assay buffer which contains 20 mM Tris, 6 mM $MgCl_2$, 1 mM $CaCl_2$, pH 7.4. The density of nuclear suspension was normalized to 1 mg DNA/ml. PARP reaction was initiated by the addition of NAD^+ stock solution to nuclear suspension to 0.5 mM NAD^+ final concentration. The reaction proceeded for 10 min (37 °C) and was stopped by nuclei withdrawal from reaction mixture by centrifugation at 13,000 *g*, 1 °C for 2 min. The supernatants were transferred to the wells of Falcon UV–Vis transparent 96-well plate. NAD^+ quantification was performed in supernatant aliquots by sequential addition of 2 M KOH and 20% acetophenone (in EtOH), yielding final concentrations of KOH, acetophenone, and formic acid in accordance with original assay. The absorbance of PARP assay buffer containing 0.5 mM NAD^+ was determined at 378 nm alongside with the samples derived from nuclear suspensions and was set as standard. The amount of NAD^+ present in samples of nuclear suspensions in PARP assay buffer was determined by subtraction of test sample absorbance from the standard. PARP 1 activity was defined as NAD^+ consumed by nuclei in 10 min.

DNA electrophoresis and DNA fragmentation assay

About 100 µl samples of nuclear suspension normalized to1 mg/ml DNA were transferred to the Ependorf tubes and 60 mM $MgCl_2$ and 10 mM $CaCl_2$ were added to yield final concentrations of 6 mM $MgCl_2$ and 1 mM $CaCl_2$ in probes. The ions were added to activate endogenous Mg^{2+}- and Ca^{2+}/Mg^{2+}-dependent nuclear endonucleases, which initiated internucleosomal DNA cleavage. DNA isolation and electrophoresis was performed according to standard protocols (Sambrook & Russell, 2001). Gels were stained with 10 mkg/ml ethidium bromide for 10 min. DNA was subjected to electrophoresis in 1.8% agarose gels (8v/cm). DNA bands were visualized by ethidium bromide staining and DNA fragmentation was assessed after gel densitometry using Fuji Film Image Gauge ver.3.12 program for determination of relative content of DNA fragments. DNA content in each band was estimated and the ratio to total DNA introduced into gel per lane was calculated (total DNA content per lane was set as 100%).

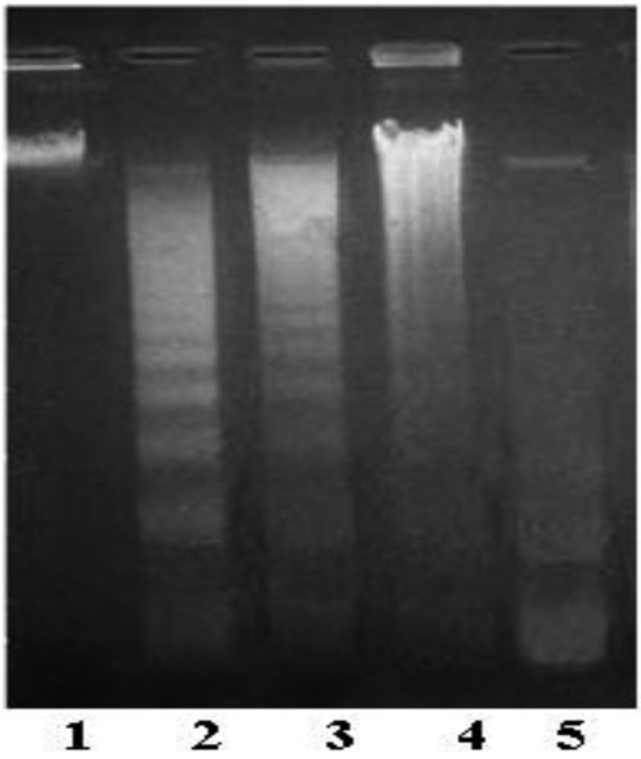

Figure 2. DNA internucleosomal fragmentation in liver nuclei incubated for 60 min in the presence of $NAD^+$and NA. 1 – Mg^{+2} and Ca^{+2} ions in incubation media, 2 – isolated nuclei incubated with 6 mM $MgCl_2$ and 1 mM Ca Cl_2, 3 – isolated nuclei incubated with 6 mM $MgCl_2$ and 1 mM $CaCl_2$ and 0.5 mM NAD^+, 4 – isolated nuclei incubated with 6 mM $MgCl_2$ and 1 mM $CaCl_2$ and 5 mM NAD^+, 5 – nuclei incubated with 6 mM $MgCl_2$, 1 mM $CaCl_2$ and 0.1 mM NA.

DNA melting

DNA concentrations were measured by spectrophotometric method, using extinction coefficient ε_{260}=6600 $M^{-1}cm^{-1}$. The ionic strength of DNA-TA solutions with $\mu = 0.02$ M was maintained by Na^+ cations. Melting of DNA–TA complexes was performed on UV/VIS PYE Unicam-SP8-100 (UK), the heating of thermostat-controlled cell (3 ml) was carried out, employing SP 876 Series 2 program device. The length of the optic pathway was 1 cm.

Melting of DNA–TA complexes was performed as described earlier (Vardevanyan, Antonyan, Parsadanyan, Torosyan, & Karapetyan, 2016) at the maximum wavelength of 260 nm. The ratio of TA and DNA concentrations varied in mentioned

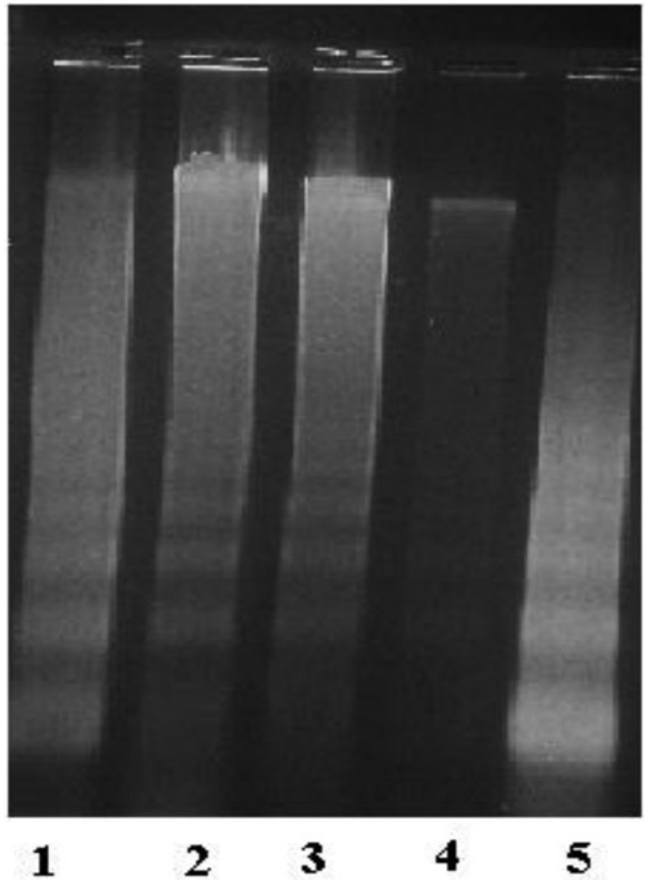

Figure 3. DNA internucleosomal fragmentation in liver nuclei isolated from liver of rats treated with TA. 1 – nuclei isolated from rats of control group incubated with 6 mM $MgCl_2$ and 1 mM $CaCl_2$, 2 – nuclei isolated from rats of control group were pre-incubated with TA 15 min and incubated 60 min with 6 mM $MgCl_2$ and 1 mM $CaCl_2$, 3 – nuclei isolated from rats in 2 h after i.p. injection of TA and incubated with 6 mM $MgCl_2$ and 1 mM $CaCl_2$ 60 min; 4 – nuclei isolated from rats in 24 h after i.p. injection of TA and incubated with 6 mM $MgCl_2$ and 1 mM $CaCl_2$ 60 min; 5 – nuclei isolated from rats in 48 h after i.p. injection of TA and incubated with 6 mM $MgCl_2$ and 1 mM $CaCl_2$ 60 min.

Table 2. Relative content of different length fragments of DNA isolated from nuclei incubated in the presence of divalent ions and different concentrations of NAD and NA. DNA content per lane in gel was set as 100%. $p^*<0.05$.

Fragment length–	60 min incubation with 6mM $MgCl_2$ and 1 mM Ca Cl_2	60 min incubation with 6mM $MgCl_2$, 1 mM Ca Cl_2 and 0.5 mM NAD^+	60 min incubation with 6mM $MgCl_2$, 1 mM Ca Cl_2 and 5mM NAD^+	60 min incubation with 6mM $MgCl_2$, 1 mM $CaCl_2$ and 0.1 mM NA
>1000 b.p.	33.9 ± 3.4	35.9 ± 0.3	54.5*±0.7	0
1000–200 b.p.	27.8 ± 0.2	20.2 ± 0.2	19.5 ± 0.5	45.3*±5.0
<200 b.p.	38.3 ± 0.1	43.9 ± 0.4	26 ± 0.2	54.7*±5.0

Table 3. Relative content of DNA (%) with different length fragments, isolated from liver nuclei of rats treated with TA. DNA content per lane in gel was set as 100%. $p < 0.05$.

Fragment length	60 min incubation with 6 mM $MgCl_2$ and 1 mM $Ca\ Cl_2$	Control group nuclei 15 min TA + 60 min incubation with 6 mM $MgCl_2$ and 1 mM $Ca\ Cl_2$	2 h after TA injection 60 min incubation with 6 mM $MgCl_2$ and 1 mM $Ca\ Cl_2$	24 h after TA injection 60 min incubation with 6 mM $MgCl_2$ and 1 mM $Ca\ Cl_2$	48 h after TA injection 60 min incubation with 6 mM $MgCl_2$ and 1 mM $Ca\ Cl_2$
>1000 b.p.	38.8 ± 3.4	35.3 ± 0.3	30.3 ± 0.3	0	15.1 ± 0.3
1000–200 b.p.	30.8 ± 1.0	56.3 ± 0.2	53.3 ± 0.2	0	50.1 ± 1.2
<200 b.p.	30.4 ± 0.1	8.4 ± 0.1	16.4 ± 0.1	100	34.8 ± 1.0

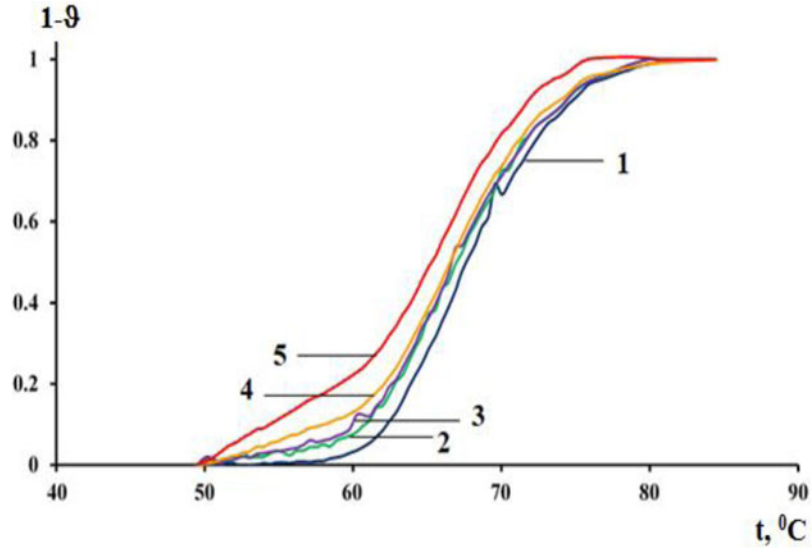

Figure 4. Melting curves of DNA (1) and TA-DNA (2-5) complexes. The ratio of TA concentration to DNA was equal to: 2 – 0.02; 3 – 0.04; 4 – 0.1; 5 – 0.2. The concentration of DNA in all examined samples was $\sim 7.5 \times 10^{-5}$ M.

Table 4. Melting temperature (T_m) and melting interval width (ΔT) of TA–DNA complexes.

TA/DNA ratio	T_m, °C	ΔT, °C
0	67.1	14.0
0.02	66.9	14.7
0.04	66.8	15
0.10	66.5	15.3
0.20	65.5	16.3

intervals: r=TA/DNA – 0; 0.02; 0.04; 0.1, and 0.2 (per base pair). The heating rate of the thermostat-controlled cell was 0.5 °C/min and the temperature was automatically recorded in every 60 s. Data emerged on PC monitor employing LabVIEW software. Temperature and absorption data were modified and saved with Microsoft Excel Office 10 software package. Absorption spectra of TA and complexes TA–DNA were recorded in wavelength interval 220" $\leq \lambda \leq$ 400 nm.

Statistical analysis

Data are expressed as mean ± s.d. Statistical differences in the results between groups were evaluated by the Student's *t*-test. A probability (p) value of <0.05 was considered significant.

Results

Addition of $Ca^{2+}$and Mg^{2+}ions into incubation media of naked liver cell nuclei led to the activation of endogenous CME which resulted in characteristic apoptotic DNA internucleosomal fragmentation. Examination of DNA fragmentation in liver nuclei isolated from control rats incubated in the presence of $Ca^{2+}$and Mg^{2+} ions revealed that internucleosomal fragmentation of DNA developed in 30 min, though low weight fragments corresponding to mono-, di-, and tri-nucleosomes are poorly visible (Table 1). This pattern of DNA laddering in control nuclei did not change in further 30 min though intensity of fragmentation increase (Figure 1, lanes 3, 4, and 5).

Evaluation of data presented in Figure 2 and Table 2 comes to show, that intensity of internucleosomal DNA fragmentation in liver nuclei incubated with NAD^+ changes in a concentration-dependent manner and was dramatically inhibited by PARP 1 inhibitor NA. This results are in good agreement with data reported by Yoshihara et al., which in 1975 established that nucleolytic activity of purified CME, assessed by the rate of free nucleotide production, was severely inhibited by NAD^+ and was stimulated by NA due to negative regulation of the endonuclease activity by poly (ADP-ribos)ylation (Yoshihara, Tamigawa, Burzio, & Koide, 1975).

The electrophoregram of DNA isolated from liver nuclei, of rats in different time intervals after i.p. injection of TA is presented in Figure 3. It is apparent that in 24 h after TA injection into rats DNA internucleosomal fragmentation in liver nuclei was stimulated. However, in 48 h after TA administration to rats, the intensity and the pattern of DNA cleavage were restored (Table 3).

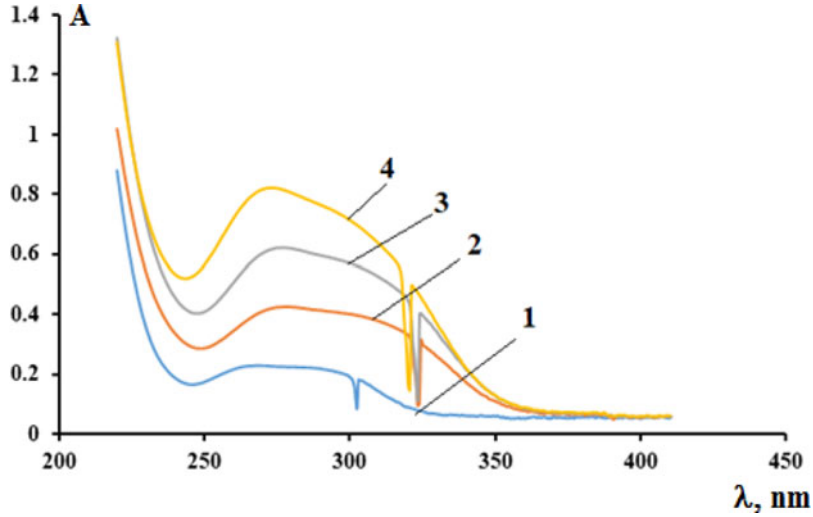

Figure 5. Absorption spectra of TA solutions with different concentrations: 1 – 1.5×10^{-6} M; 2 – 3×10^{-6} M; 3 – 7.5×10^{-6} M; 4 – 1.5×10^{-5} M.

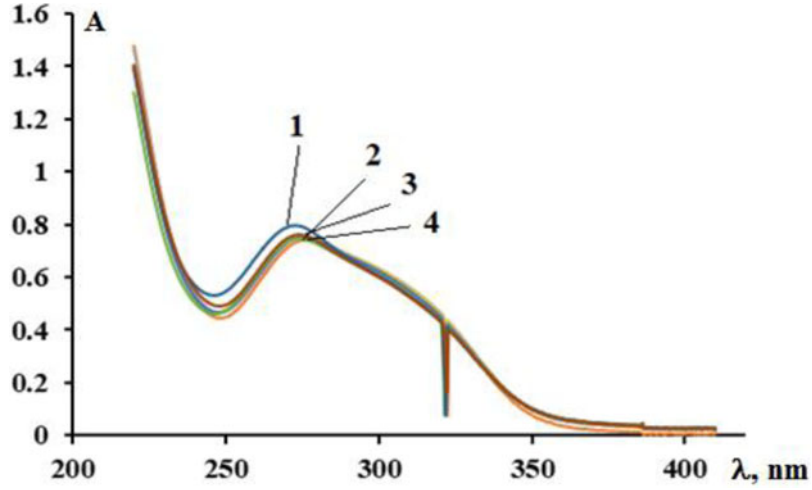

Figure 6. Absorption spectra of TA-DNA complexes containing $\sim 10^5$ M TA and different concentrations of DNA: 1 – 0 M DNA; 2 – 8.5×10^{-6} M DNA; 3 – 1.7×10^{-5} M DNA; 4 – 3.4×10^{-5} M DNA.

The data, presented in Figure 4, demonstrate that melting curves of TA-DNA complexes are shifted towards low temperatures. Moreover, the higher is the concentration of TA, the more expressed is the shift to the lower temperatures. From the melting curves (Figure 4) as well as from the results summarized in Table 4, it is obvious that the decrease in T_m was paralleled with the increase in ΔT (melting interval width). Considering that melting profiles of TA–DNA complexes could result from interference with absorption spectra either TA or DNA, we examined absorption of TA and DNA solutions in wavelength interval $220 \leq \lambda \leq 400$ nm.

It was found that the UV/VIS spectrum of TA is characterized with a broad interval of maximum absorption between $\lambda = 275.5$ and $\lambda = 325.5$ nm (Figure5). From the absorption spectra (Figure 5) one can conclude that the absorption interval of TA interferes in some degree with that of DNA, which can result to the melting changes of TA-DNA complexes described in Figure 4.

Spectrophotometric titration of TA with DNA was performed versus DNA solutions with the same concentrations of DNA solutions that were employed in titration procedure (Figure 6).

Discussion

It is widely accepted that chromatin condensation is a serious obstacle to the realization of transcription, DNA replication and DNA repair. Alterations in this basic chromatin associated nuclear functions underlie tumorogenesis and many pathologic states. The role of PARP1 activation is firmly established in regulation of local and general chromatin structure and in all aforementioned chromatin-associated functions (Gupte, Liu, & Kraus, 2017). Currently, PARP 1 inhibitors (PARPi) are employed in treatment of cancer patients (O'Sullivan, Chen, Meehan, & Doroshow, 2017). The vast majority of PARPi presents NAD^+-competing substrates. However, PARPi resistance challenges curative potential of this chemotherapeutic approach. The analysis of PARPi resistance mechanisms revealed that endogenous PARG activity is

crucial for the success of PARPi based therapy (Francica & Rottenberg, 2018).

PARG is an enzyme that is implicated in major mechanism limiting PARylation of proteins. Hydrolysis of PAR chains linked to auto-modification domain of PARP 1 is essential for maintaining PARP 1 activity in the cell. Coming from this, inhibition of PARG is considered as promising strategy for PARP 1 inhibition and search of PARG inhibitors is in progress.

A large body of evidence indicates on the high potential of TA to inhibit PARG activity and its anti-cancer activity (Zhang, Li, Kim, Hagerman, & Lü, 2009). Here, employing animal model, we study the effect of treatment of rats with TA on chromatin condensation in liver nuclei in different time intervals after i.p. injection of TA.

It is well established that nuclear Ca^{2+}/Mg^{2+}-dependent endonuclease (CME) participates in apoptotic internucleosomal DNA fragmentation. The pattern of internucleosomal DNA cleavage and its intensity are used as a measure of chromatin condensation in cell nuclei (Widlak, Li, Wang, & Garrard, 2000). We applied the method of artificial activation of CME to assess condensation of chromatin in liver cell nuclei of rats that underwent treatment with TA.

Our results come to show that treatment of rats with TA stimulated DNA internucleosomal fragmentation which indicated on increased accessibility of liver chromatin to CME in 24 h after TA injection into animals. In 48 h after TA injection into rats, liver chromatin tends to restore the basal level of condensation. These data indicate on TA-induced dynamic decondensation of chromatin. We speculate that transient decondensation of chromatin could result from lengthening of PAR chain attached to PARP 1 auto-modification domain and decrease of over-PARylated PARP-1 affinity to DNA (Kim, Mauro, Gévry, Lis, & Kraus, 2004) due to TA-induced PARG inhibition.

Taking into account that chromatin condensation could depend on modification of axial structural component of chromatin, i.e. DNA, we study whether TA possesses the capability to affect the structure of calf thymus DNA. In this purpose, we examine absorption curves of TA, TA–DNA complexes, and melting curves of TA–DNA complexes.

Data of this set of experiments come to show that TA absorption spectra exhibit a broad interval of maximum between $260< \lambda <320$ nm, without existence of sharp absorption peak. We suppose that this broad interval of maximal absorption could evidence more than one chromophore group in TA molecule. It was apparent that absorption spectra of TA–DNA complexes did not significantly differ from TA spectra. In contrast, melting curves of DNA and TA–DNA complexes demonstrate marked differences. The values of T_m of TA-DNA complexes decrease and the curves exhibit widening of melting interval $-\Delta T$. These data come to show that TA could directly interfere with DNA and destabilize its native structure (Karapetian, et al., 1996; Vardevanyan, Antonyan, Parsadanyan, Torosyan, & Karapetyan, 2016).

Coming from our data, we hypothesize that treatment of rats with TA could modulate chromatin structure in liver nuclei and induce transient decondensation of chromatin by two routes: first-destabilizing DNA structure, second-modulating PARylation of chromatin-associated proteins.

Conclusion

It was demonstrated that treatment of animals with TA induced transient increase of liver chromatin accessibility to Ca^{+2}/Mg^{+2}-dependent apoptotic endonuclease (CME), which evidence chromatin decondensation in 24 h after TA injection. A study of the melting curves of TA-calf thymus DNA complexes revealed that TA can induce chromatin decondensation destabilizing DNA structure.

Disclosure statement

No potential conflict of interest was reported by the authors.

Funding

This work was supported by the RA MES State Committee of Science, in the frames of the research project no. 18T-1F011.

References

Francica, P., & Rottenberg, S. (2018). Mechanisms of PARP inhibitor resistance in cancer and insights into the DNA damage response. *Genome Medicine*, *10*(1), 101. doi.org/10.1186/s13073-018-0612-8

Gupte, R., Liu, Z., & Kraus, W. L. (2017). PARPs and ADP-ribosylation: Recent advances linking molecular functions to biological outcomes. *Genes & Development*, *31*(2), 101–126. doi:10.1101/gad.291518.116

Hewish, D. R., & Burgoyne, L. A. (1973). Chromatin sub-structure. The digestion of chromatin DNA at regularly spaced sites by a nuclear deoxyribonuclease. *Biochemical and Biophysical Research Communications*, *52*(2), 504–510. doi:10.1016/0006-291X(73)90740-7

Karapetian, A. T., Mehrabian, N. M., Terzikian, G. A., Vardevanian, P. O., Antonian, A. P., Borisova, O. F., & Frank-Kamenetskii, M. D. (1996). Theoretical treatment of melting of complexes of DNA with ligands having several types of binding sites on helical and single stranded DNA. *Journal of Biomolecular Structure and Dynamics*, *14*(2), 275–283. doi:10.1080/07391102.1996.10508118

Karlberg, T., Langelier, M.-F., Pascal, J. M., & Schüler, H. (2013). Structural biology of the writers, readers and erasers in mono and poly(ADP-ribose) mediated signalling. *Molecular Aspects of Medicine*, *34*(6), 1088–1108. doi:10.1016/j.mam.2013.02.002

Kim, M. Y., Mauro, S., Gévry, N., Lis, J. T., & Kraus, W. L. (2004). NAD^+-dependent modulation of chromatin structure and transcription by nucleosome binding properties of PARP-1. *Cell*, *119*(6), 803–814. doi:10.101/j.cell.2004.11.002

Longelier, M. F., Planck, J. L., Roy, S., & Pascal, J. M. (2012). Structural basis for DNA damage-dependent poly(ADP-riboyl)ation by human PARP-1. *Science*, *336*, 728–732. doi:10.1126/science.1216338

O'Sullivan, G. C., Chen, A. P., Meehan, R., & Doroshow, J. H. (2017). PARP inhibitors in reproductive system cancers. *Drugs*, *77*, 113–130. doi:10.1007/s40265-016-0688-7

Putt, K. S., & Hergenrother, P. J. (2004). An enzymatic assay for poly(ADP – ribose) polymerase – 1 (PARP-1) via the chemical quantitation of NAD^+: Application to the high-throughput screening of small molecules as potential inhibitors. *Analytical Biochemistry*, *326*(1), 78–86. doi:10.1016/j.ab.2003.11.015

Sambrook, J., & Russell, D. W. (2001). *Molecular cloning* (3 ed.). Cold Spring Harbor, NY: Cold Spring Harbor Laboratory Press. https://www.worldcat.org/title/molecular-cloning-a-laboratory-manual/oclc/45015638

Tanuma, S., Sakagami, H., & Endo, H. (1989). Inhibitory effect of tannin on poly(ADP-ribose)glycohydrolase from human placenta. *Biochemistry International*, *18*(4), 701–708. PMID 2764971.

Vardevanyan, P. O., Antonyan, A. P., Parsadanyan, M. A., Torosyan, M. A., & Karapetian, A. T. (2016). Joint interaction of Ethidium Bromide and

Methylene Blue with DNA. The effect of ionic strength on binding thermodynamic parameters. *Journal of Biomolecular Structure and Dynamics*, *34*(7), 1377–1382. doi:10.1080/07391102.2015.1079557

Widlak, P., Li, P., Wang, X., & Garrard, W. T. (2000). Cleavage preferences of the apoptotic endonuclease DFF40 (Caspase-activated DNase or Nuclease) on naked DNA and chromatin substrate. *Journal of Biological Chemistry*, *275*(11), 8226–8232. doi:10.1074/jbc.275.11.8226

Yoshihara, K., Tanigawa, Y., Burzio, L., & Koide, S. S. (1975). Evidence for adenosine diphosphate ribosylation of Ca^{2+}, Mg^{2+}-dependent endonuclease. *Proceedings of the National Academy of Sciences*, *72*(1), 289–293. doi:10.1073/pnas.72.1.289

Zhang, J., Li, L., Kim, S. H., Hagerman, A. E., & Lü, J. (2009). Anti-cancer, anti-diabetic and other pharmacologic and biological activities of penta-galloyl-glucose. *Pharmaceutical Research*, *26*(9), 2066–2080. doi:10.1007/s11095-009-9932-0